Supplementary Information

Weaving host matrixes with intermolecular hydrogen bonds for high-efficiency white thermally activated delayed fluorescence

Yuee Tian‡, Huiqin Wang‡, Yi Man, Nan Zhang, Jing Zhang*, Ying Li, Chunmiao Han and Hui Xu*

Key Laboratory of Functional Inorganic Material Chemistry, Ministry of Education & School of Chemistry and Material Science, Heilongjiang University, 74 Xuefu Road, Harbin 150080, P. R. China.
E-mail: zhangjing@hlju.edu.cn; hxu@hlju.edu.cn

Content

I. Experimental Section

Materials and Instruments

The reagents and solvents used for the synthesis were purchased from Aldrich and Alfa-Aesar companies and used without further purification. DMAC-DPS was purchased from p-OLED company and used directly. **DPEQPO** was prepared according to our previous report.[1] CCDC number of **DPEQPO** is CCDC 2100434.

^{1}H NMR spectra were recorded using a Varian Mercury plus 400NB spectrometer relative to tetramethylsilane (TMS) as internal standard. Molecular masses were determined by a FINNIGAN LCQ Electro-Spraying Ionization-Mass Spectrometry (ESI-MS), or a MALDI-TOF-MS. Elemental analyses were performed on a Vario EL III elemental analyzer. The crystal suitable for single-crystal XRD analysis was obtained through slowly diffusing hexane into dichloromethane solution of **DPXQPO** at room temperature. All diffraction data were collected at 295 K on a Rigaku Xcalibur E diffractometer with graphite monochromatized Mo Kα (λ = 0.71073 Å) radiation in ω scan mode. All structures were solved by direct method and difference Fourier syntheses. Non-hydrogen atoms were refined by full-matrix least-squares techniques on F2 with anisotropic thermal parameters. The hydrogen atoms attached to carbons were placed in calculated positions with C−H = 0.93 Å and U(H) = 1.2Ueq(C) in the riding model approximation. All calculations were carried out with the SHELXL97 program. Thermogravimetric analysis (TGA) and differential scanning calorimetry (DSC) were performed on Shimadzu DSC-60A and DTG-60A thermal analyzers under nitrogen atmosphere at a heating rate of 10 °C min^{-1}. Cyclic voltammetric (CV) studies were conducted using an Eco Chemie B. V. AUTOLAB potentiostat in a typical three-electrode cell with a platinum sheet working electrode, a platinum wire counter electrode and a silver/silver chloride (Ag/AgCl) reference electrode. Tetrabutylammonium hexafluorophosphate was used as electrolyte with a concentration of 0.1 mol L^{-1}. All electrochemical experiments were carried out under a nitrogen atmosphere at room temperature in dichloromethane. Steady-state and time-resolved emission spectra were recorded with an Edinburgh FLS 1000 fluorescence spectrophotometer, based on time-correlated single photon counting (TCSPC) method with a nanosecond and a microsecond pulsed light sources. The film samples used for measurement were prepared

through *vacuum* evaporation. η_{PL} was evaluated with a labsphere 1-M-2 (ϕ = 6") integrating sphere coated by Benflect with efficient light reflection in a wide range of 200-1600 nm. Ultraviolet Photoelectron Spectra (UPS) measurements were carried out with a Shimadzu/Kratos Axis Ultra DLD spectrometer, using the HeI radiation (21.21 eV) from a He discharge lamp. Peaks were recorded with constant pass energy of 5 eV and the step size of 0.05 eV. The pressure in the analysis chamber was around 4.3×10^{-9} torr. The instrument was operated in a mode that yielded a Fermi-level width of 0.4 eV for Ag metal and at a full width a half maximum of 0.54 eV for Ag 3d5/2 core level peak. Energy scale was calibrated using the Fermi level of clean Ag.

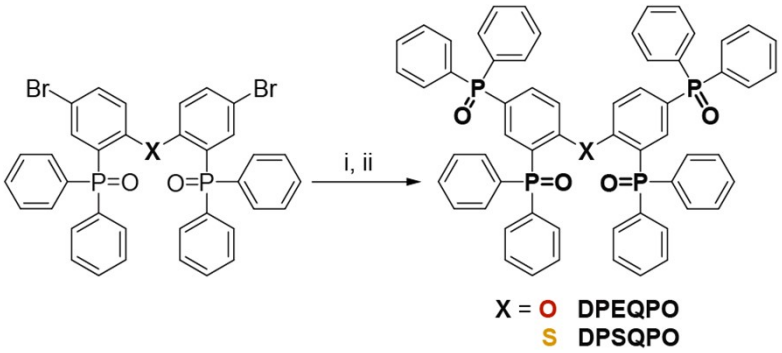

Scheme S1. Synthetic procedure of **DPXQPO**. i. $DPSDPOBr_2$, NaOAc, $Pd(OAc)_2$, $PHPh_2$, DMF, 130 °C, 24 h; ii. 30% H_2O_2, CH_2Cl_2, 0 °C, 4 h.

Synthesis method

(Thiobis(benzene-4,1,3-triyl))tetrakis(diphenylphosphine oxide) (DPSQPO): In Ar, (thiobis(5-bromo-2,1-phenylene))bis(diphenylphosphine oxide) ($DPSDPOBr_2$, 0.746 g, 1 mmol), diphenylphosphine (0.5 mL, 3 mmol), $Pd(OAc)_2$ (5 mg, 0.002 mmol) and NaOAc (0.246 g, 3 mmol) were added in N,N'-dimethyl formamide (DMF, 5 ml), and heated to 130 °C. The mixture was stirred for 24 h. The system was then cooled to room temperature and poured into water. The mixture was extracted with dichloromethane (3 × 10 ml). The combined oil phase was concentrated to 10 mL, and then cooled to 0 °C. The mixture was added with 30% hydrogen peroxide (0.7 ml, 5 mmol) in dropwise. After reacting for 4 h, the system was extracted with water and dichloromethane (3 × 10 ml). The organic layer was combined and dried with anhydrous Na_2SO_4.The solvent was removed in *vacuo*, and the residue was purified by flash column chromatography to give

the white powder of 0.730 g with a yield of 74%.

^{1}H NMR (TMS, $CDCl_3$, 400 MHz): δ = 7.698-7.650 (m, 2H), 7.526-7.468 (m, 20H), 7.431-7.347 (m, 14H), 7.343-7.272 (m, 9H), 7.085-7.052 ppm (m, 2H); LDI-MS: m/z (%): 986 (100) [M^+]; elemental analysis (%) for $C_{60}H_{46}O_4P_4S$: C 73.02, H 4.70; found: C 73.04, H 4.72. CCDC Number: CCDC2100433.

Theoretical calculation

The ground state and singlet and triplet excited states in vacuum were simulated on the basis of single crystal data by the restricted and unrestricted formalism of Beck's three-parameter hybrid exchange functional[2] and Lee, and Yang and Parr correlation functional[3] B3LYP/6-31G(d,p), respectively. The total energies were also corrected by zero-point energy. TDDFT simulation for natural transition orbital (NTO) analysis was performed on the basis of optimized ground-state geometries at the level of ωB97XD/6-31G(d,p).[4] The contours were visualized with Gaussview 5.0. All computations were performed using the Gaussian 09 package.

Fabrication and characterization of OLEDs

ITO substrate was cleaned with detergents and deionized water, dried in an oven at 120 °C for 4 h, treated with oxygen plasma for 3 min, and then transferred to a deposition chamber. Devices were fabricated by evaporating each layer onto ITO substrate sequentially at a pressure below 1×10^{-6} Tor. A MoO_3 layer was first deposited on ITO substrate at 0.1 nm s^{-1}. The deposition rates of organic layers were 0.1-0.3 nm s^{-1}. Then, a 1nm layer of LiF was deposited at 0.1 nm s^{-1}. Finally, a 100-nm-thick layer of Al was deposited at 0.6 nm s^{-1} as the cathode. The devices were then transferred to glovebox and encapsulated with hot melt glue. The emission areas of the devices were 0.09 cm^2. The EL spectra were measured with a PR655 spectra colorimeter. The current-density-voltage and brightness–voltage curves of the devices were measured using a Keithley 4200 source meter and a calibrated silicon photodiode. All the measurements were carried out in atmosphere.

II. Single Crystal Structure

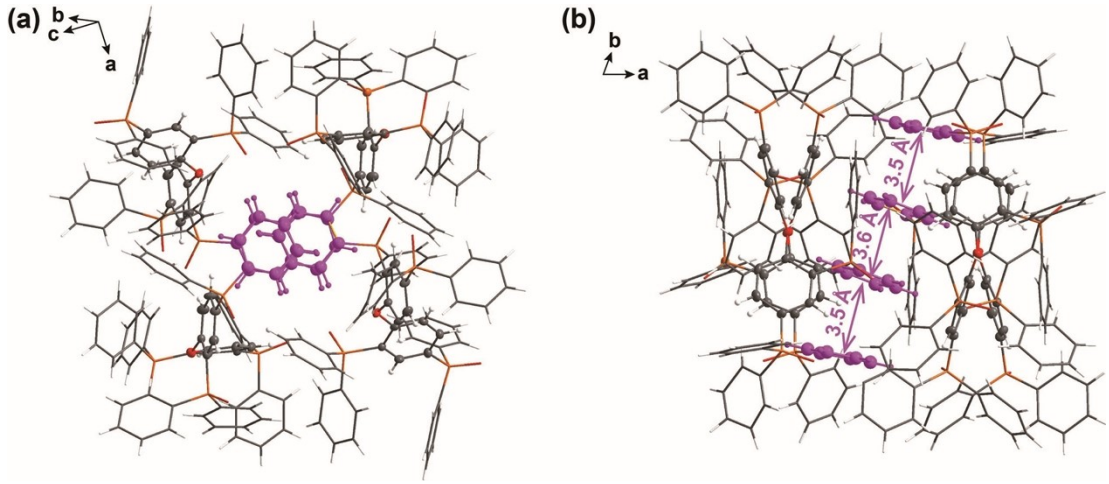

Figure S1. Single crystal packing diagram of **DPEQPO**. The intramolecular π-π interaction and hydrogen bonds are highlighted with blue and purple dash lines.

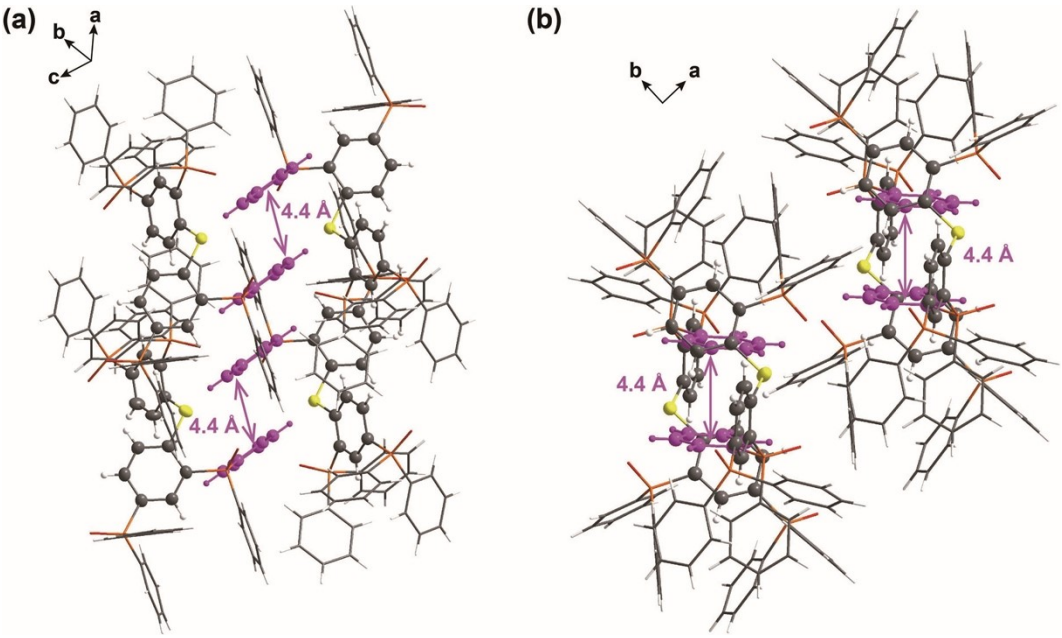

Figure S2. Single crystal packing diagram of **DPSQPO**. The intramolecular π-π interaction and hydrogen bonds are highlighted with blue and purple dash lines.

III. Morphological Properties

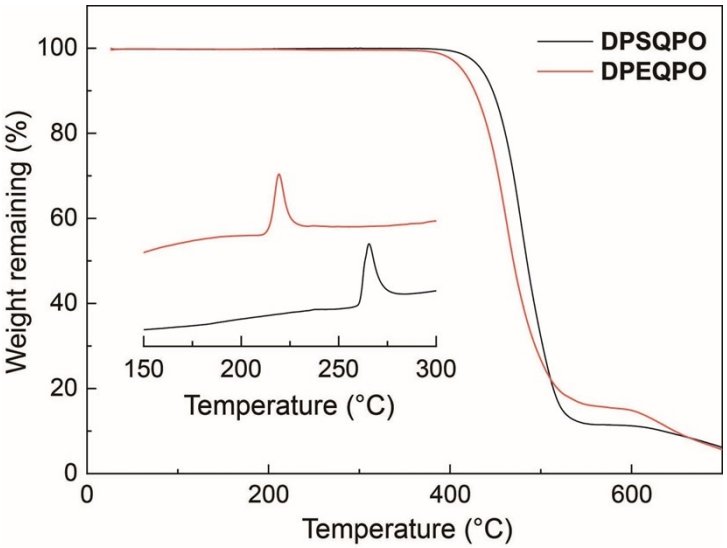

Figure S3. DSC and TGA curves of **DPSQPO** and **DPEQPO**.

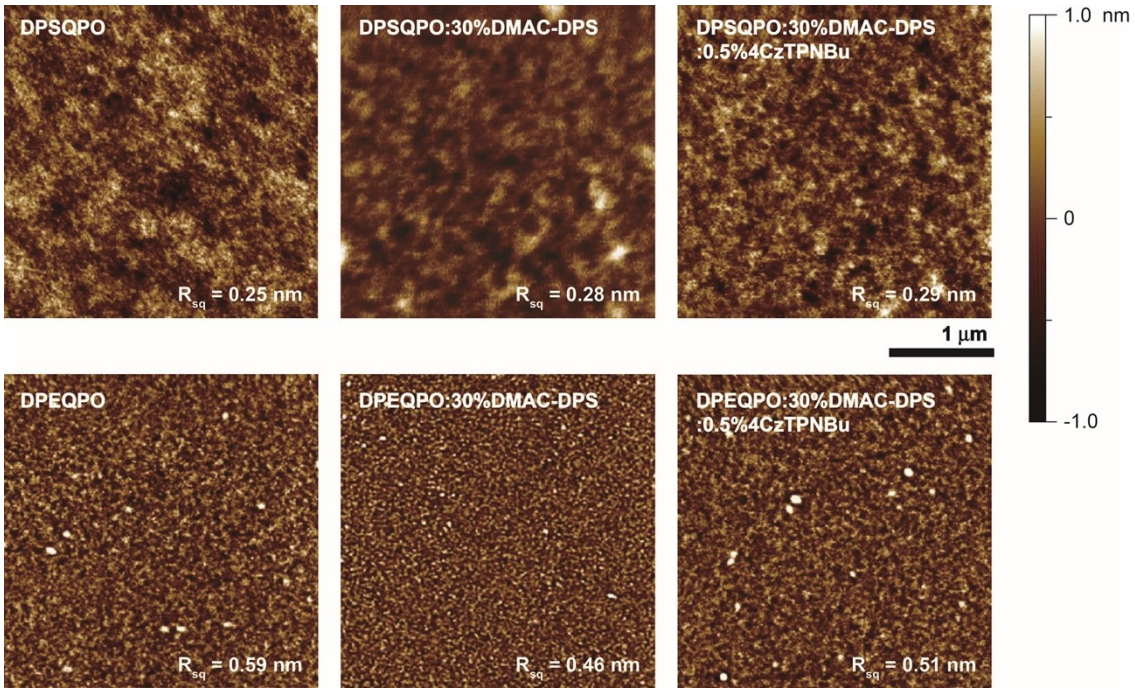

Figure S4. AFM images of *vacuum*-evaporated **DPSQPO** and **DPEQPO** based films (100 nm).

VI. EL Performance of DPXQPO-Based Blue and White TADF Diodes

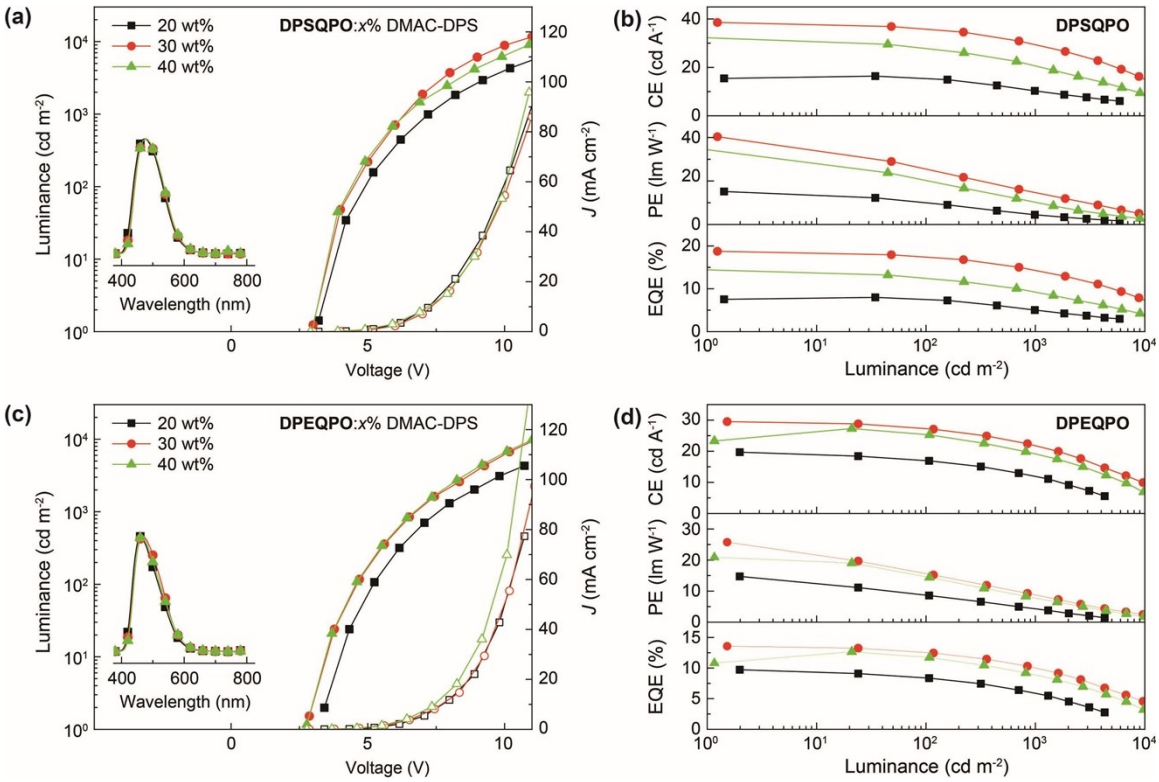

Figure S5. Current density (*J*)-voltage-luminance characteristics and EL spectra (inset) of **DPSQPO** (a) and **DPEQPO** (c) based blue-emitting devices; Current efficiency (CE), power efficiency (PE) and external quantum efficiency (EQE)-Luminance curves of the devices based on **DPSQPO** (b) and **DPEQPO** (d).

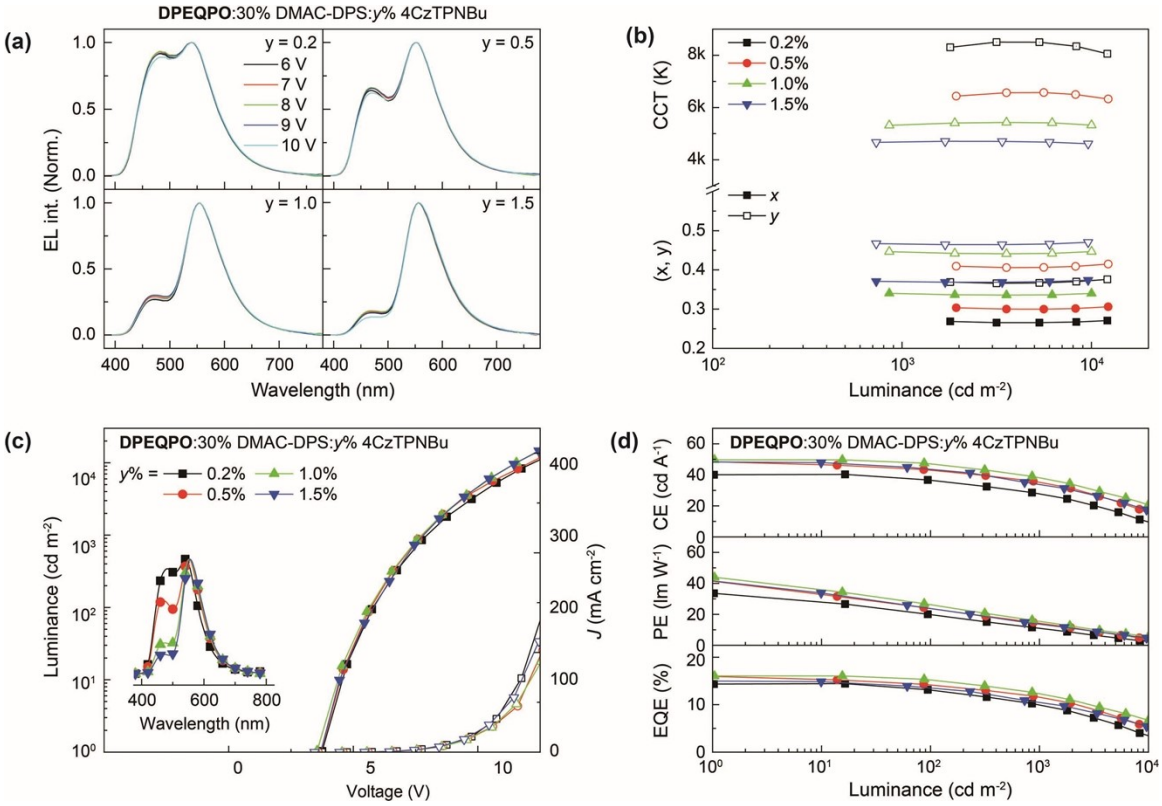

Figure S6. Dependence of current density (*J*)-voltage-luminance characteristics and EL spectra (inset) of **DPSQPO** (a) and **DPEQPO** (c) based WOLEDs on the doping concentration of 4CzTPNBu; influence of 4CzTPNBu concentrations on current efficiency (CE), power efficiency (PE) and external quantum efficiency (EQE)-Luminance curves of **DPSQPO** (b) and **DPEQPO** (d) based WOLEDs.

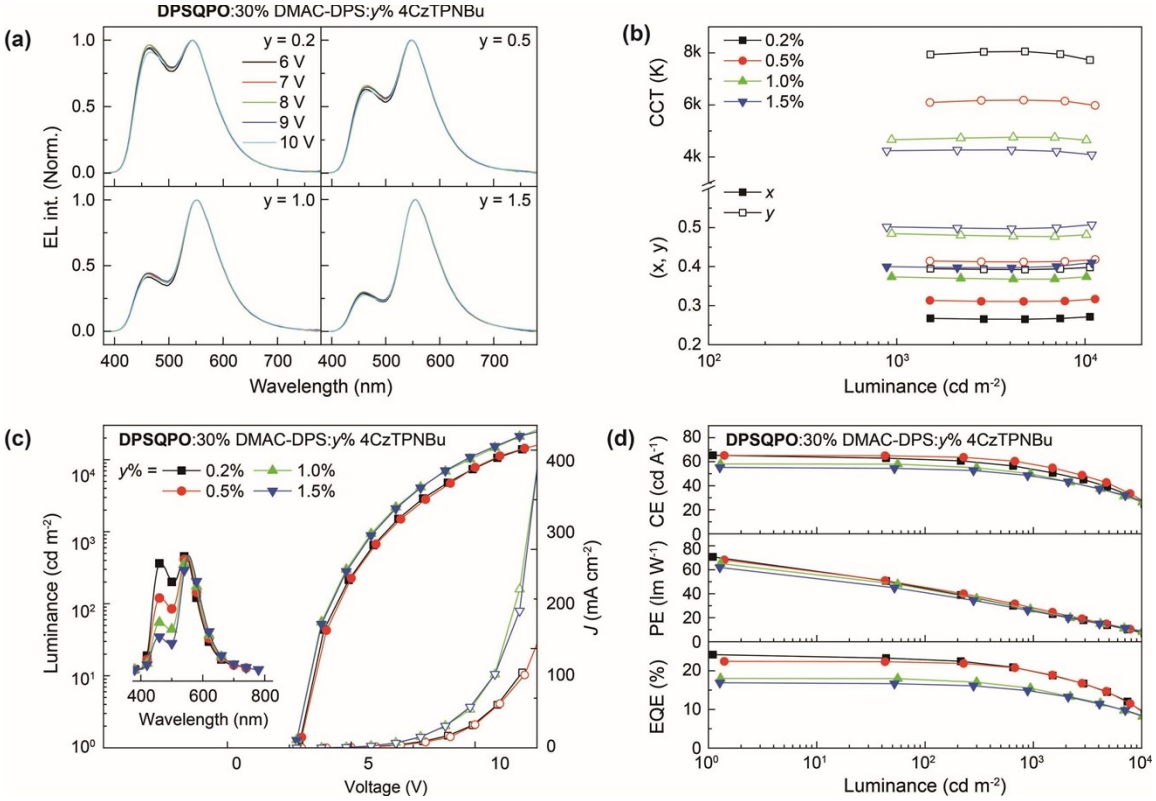

Figure S7. Dependence of current density (*J*)-voltage-luminance characteristics and EL spectra (inset) of **DPSQPO** (a) and **DPEQPO** (c) based WOLEDs on the doping concentration of 4CzTPNBu; influence of 4CzTPNBu concentrations on current efficiency (CE), power efficiency (PE) and external quantum efficiency (EQE)-Luminance curves of **DPSQPO** (b) and **DPEQPO** (d) based WOLEDs.

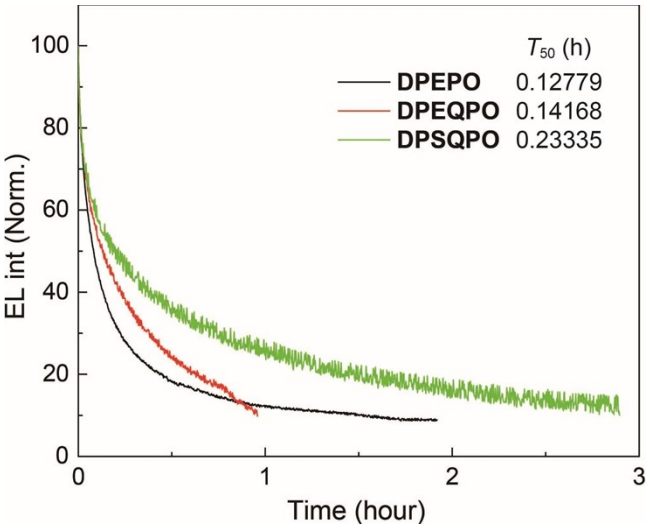

Figure S8. Comparison on device duration of **DPEPO**, **DPEQPO** and **DPSQPO**-based WOLEDs. T_{50} refers to time used at 50% luminance reduction, which were evaluated by a direct method. The devices for measurement were simply encapsulated with heat glue, and directly measured in ambient condition.

Table S1. EL performance of **DPXQPO**-hosted blue and white TADF devices.

Emissive layer	*x*/*y* (%)	V[a] (V)	L_{max}[b] (cd m^{-2})	η[c]			λ_{EL} (nm) / CIE (x, y)[d]
				η_{CE} (cd A^{-1})	η_{PE} (lm W^{-1})	η_{EQE} (%)	
DPSQPO:*x*% DMAC-DPS	20	3.2, 5.2, 7.2	5907	16.4, 14.9, 10.3	15.2, 9.0, 4.5	8.0, 7.3, 5.0	478 / (0.17, 0.27)
	30	3.0, 4.5, 6.5	12250	38.6, 36.9, 30.9	40.4, 28.9, 16.2	18.8, 17.9, 15.0	480 (0.18, 0.29)
	40	2.9, 4.4, 6.3	9065	32.4, 27.5, 22.4	35.1, 20.3, 11.9	14.5, 12.4, 10.0	480 (0.19, 0.30)
DPEQPO:*x*% DMAC-DPS	20	4.2, 6.2, 9.2	4305	19.7, 16.9, 11.1	14.7, 8.6, 3.8	9.7, 8.4, 5.5	460 / (0.17, 0.24)
	30	3.6, 5.6, 8.0	9656	29.5, 27.1, 22.4	25.7, 15.2, 9.3	13.6, 12.5, 10.3	464 / (0.18, 0.26)
	40	3.5, 5.5, 8.0	9767	27.3, 25.3, 19.9	20.9, 14.4, 8.3	12.7, 11.7, 9.2	468 / (0.17, 0.27)
DPSQPO:30% DMAC-DPS:*y*% 4CzTPNBu	0.2	2.9, 4.2, 6.2	13940	65.3, 61.7, 56.4	70.8, 48.6, 30.0	24.2, 22.7, 20.9	476, 540 / (0.28, 0.39)
	0.5	3.0, 4.5, 6.5	17533	65.2, 64.4, 60.4	68.2, 45.5, 31.6	22.4, 22.1, 20.7	468, 552 / (0.31, 0.41)
	1.0	2.8, 4.2, 5.8	28240	58.1, 55.9, 50.0	65.2, 42.9, 27.1	18.0, 17.5, 15.5	468, 552 / (0.37, 0.48)
	1.5	2.8, 4.2, 5.8	25843	55.2, 53.5, 48.6	61.9, 40.0, 26.3	16.9, 16.3, 14.9	468, 556 / (0.40, 0.50)
DPEQPO:30% DMAC-DPS:*y*% 4CzTPNBu	0.2	3.7, 5.8, 7.8	12140	40.3, 36.8, 28.5	33.6, 20.1, 11.5	14.4, 13.2, 10.2	464, 544 / (0.27, 0.37)
	0.5	3.6, 5.6, 7.6	16890	48.7, 43.4, 35.8	42.5, 24.3, 14.8	16.0, 14.2, 11.8	464, 548 / (0.30, 0.41)
	1.0	3.6, 5.6, 7.6	20710	49.7, 47.5, 39.0	44.0, 26.8, 16.2	16.1, 15.3, 12.5	464, 552 / (0.34, 0.44)
	1.5	3.5, 5.5, 7.5	20700	48.4, 42.7, 33.2	44.1, 23.0, 14.4	15.0, 13.4, 10.5	464, 556 / (0.37, 0.47)

[a] At 1, 100 and 1000 cd m^{-2}; [b] the maximum luminance; [c] EL efficiencies at the maximum and 100 and 1000 cd m^{-2}; [d] peak wavelengths and CIE coordinates of EL emissions at 1000 cd m^{-2}.

Table S2. EL performance of representative TADF white OLEDs**.**

Emissive layer	V[a] (V)	L_{max}[b] (cd m^{-2})	η[c]			λ_{EL} (nm) / CIE (x, y)[d]	Ref.
			η_{CE} (cd A^{-1})	η_{PE} (lm W^{-1})	η_{EQE} (%)		
TrisPCz|mCBP:4CzPN|mCBP:4CzPN :4CzTPN-Ph|PPT:3CzTRZ	3.6, 5.4, 7.8	~4000	45.6, 32.4, 20.6	34.1, 18.8, 8.3	17.0, 13.3, 8.5	480, 580 (0.33, 0.41)	*Appl. Phys. Lett.* **2014**, *104*, 233304
CBP:3,6-2TPA-TXO|CBP|CBP:3,6-2TPA-TX	3.4, 6.7, 9.1	-	49.5, 14.9, 8.5	48.6, 6.9, 2.9	20.4, 6.9, 1.3	470, 580 (0.32, 0.40)	*Adv. Funct. Mater.* **2016**, *26*, 6904
HATCN|TAPC|CBP:NI-1-PhTPA|CBP:PXZDSO2|CBP:NI-1-PhTPA|TmPyPB|LiF	3.6, -, -	>10000	43.3, -, 36.1	33.6, -, 17.7	15.8, -, 13.3	440, 560 (0.40, 0.48)	*Adv. Mater.* **2016**, *28*, 4614
SFXSPO:DMAC-DPS:4CzPNPh	3.9, <5.5, <7.3	~15000	50.5, 48.5, 41.4	40.6, 27.6, 17.9	19.1, 18.3, 15.7	480, 560 (0.32, 0.43)	*Adv. Mater.* **2016**, *28*, 3122
SXSPO:DMAC-DPS:4CzTPNBu	3.1, 4.8, 6.9	22430	56.7, 51.0, 43.5	57.5, 34.0, 20.1	22.1, 20.0, 17.0	468, 548 0.31, 0.39	*Chem. Eng. J.* **2019**, *374*, 471-478
CBP:FDQPXZ|DPEPO:DMAC-DPS	2.6, 2.8, 3.2	< 30000	51.3, 46.5, 31.9	59.6, 52.4, 31.7	20.5, 18.8, 13.0	480, 560 (0.33, 0.41)	*Nat Commun* **2019**, *10*, 2380.
DBFDPO:TtBCzDFTPPO:4CzTPNBu	3.1, 3.8, 5.1	20125	60.6, 55.6, 49.1	61.4, 42.5, 30.3	22.3, 20.4, 18.0	480, 544 (0.28, 0.40)	*Adv. Funct. Mater.* **2020**, *30*, 1908568
*p*tBCzPO2TPTZ:4CzTPNBu	3.1, 5.5, 7.9	37160	52.7, 51.7, 46.2	55.1, 32.4, 18.1	23.6, 23.0, 20.7	480, 560 (0.34, 0.36)	*Adv. Mater.* **2020**, *32*, 1906950
*m*CP:*pD*PBITPO:35% DMAC-DPS:0.5% 4CzTPNBu	2.9, 4.9, 7.1	36760	90.9, 84.3, 75.6	98.4, 54.0, 34.4	30.6, 28.4, 25.4	476, 564 (0.43, 0.48)	*Nat Commun* **2021**, *12*, 3640

[a] At 1, 100 and 1000 cd m^{-2}; [b] the maximum luminance; [c] EL efficiencies at the maximum and 100 and 1000 cd m^{-2}; [d] peak wavelengths and CIE coordinates of EL emissions at 1000 cd m^{-2}.

V. Gaussian Simulation Results

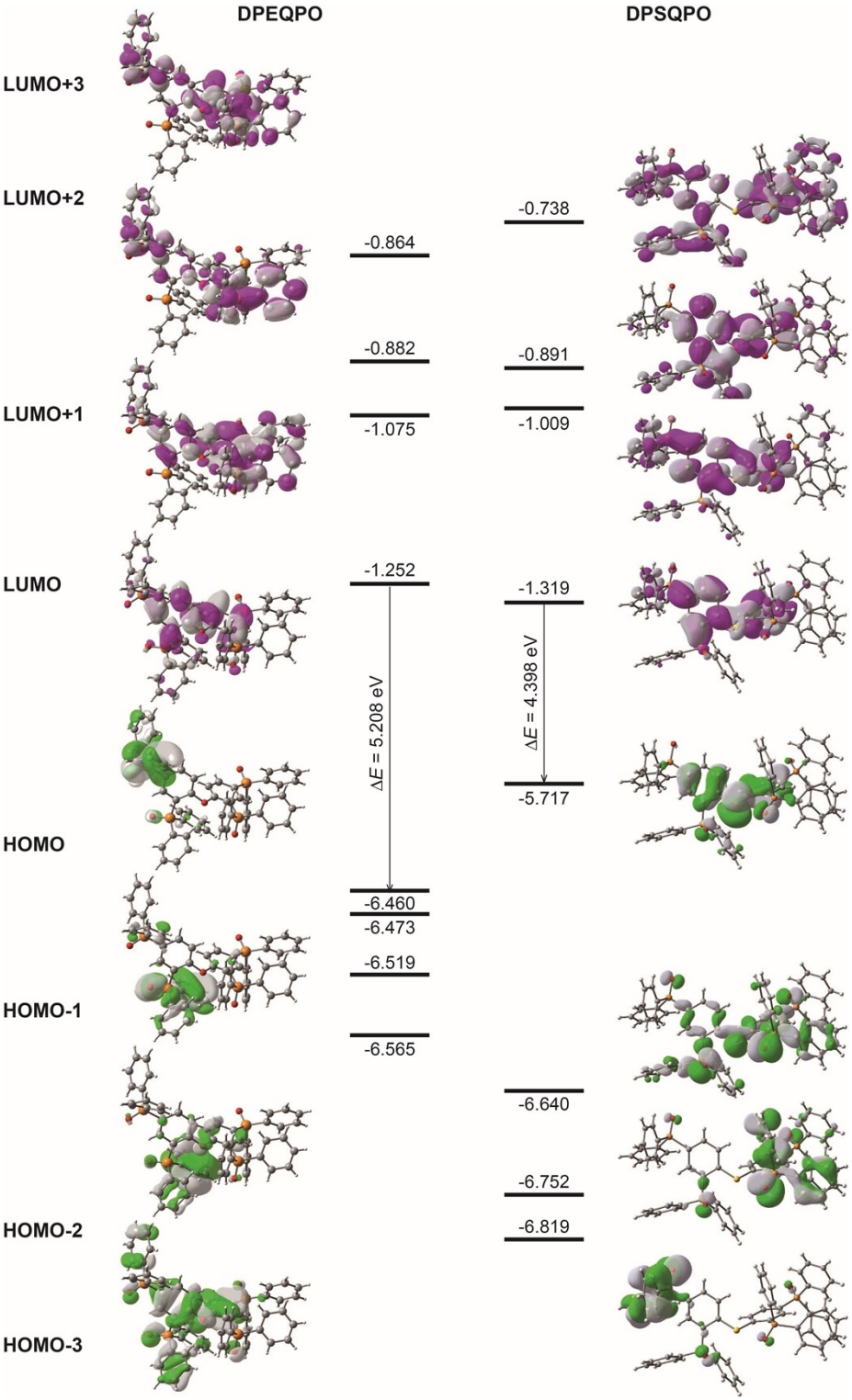

Figure S9. Frontier molecular orbital (FMO) energy levels and contours of **DPXQPO**.

VI. Electrical Properties

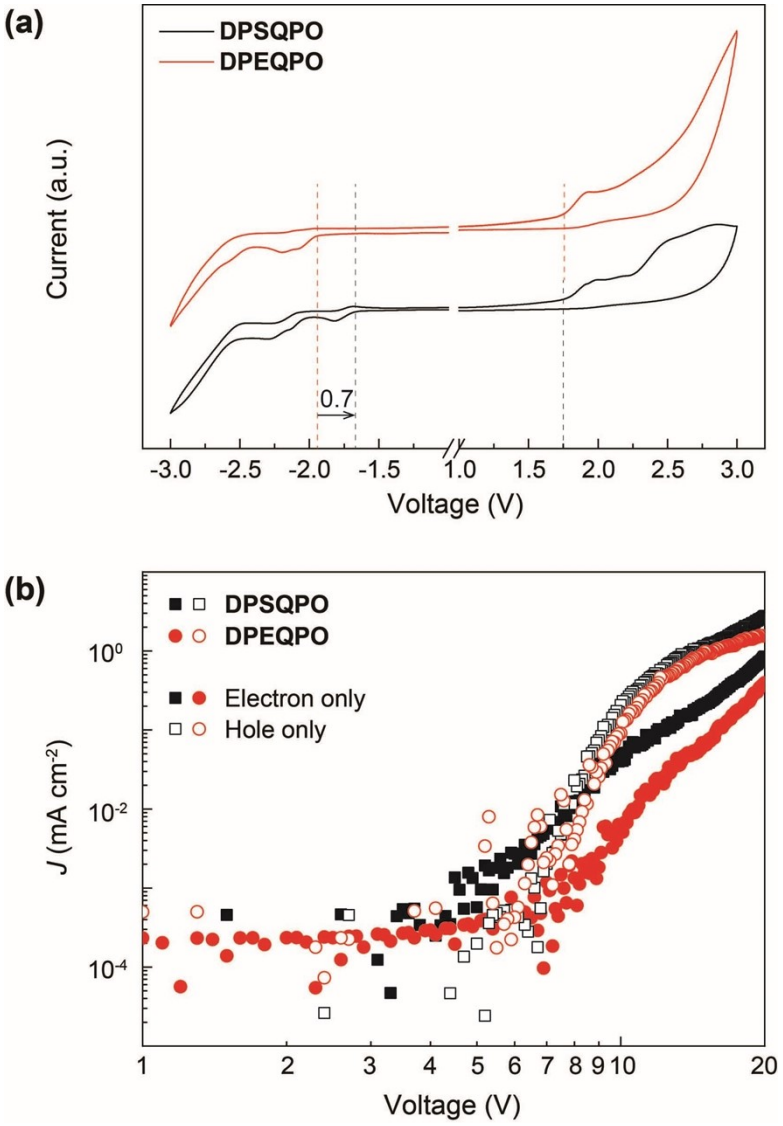

Figure S10. (a) Cyclic voltammograms of **DPXQPO** measured at room temperature with the scanning rate of 100 mV s^{-1}; (b) Voltage-current characteristics of single-carrier transporting devices based on **DPXQPO** with the structures of ITO|MoO_3 (6 nm)|**DPXQPO** (100 nm)|MoO_3 (6 nm)|Al (100 nm) for hole-only and ITO|LiF (1 nm)|**DPXQPO** (100 nm)|LiF (1 nm)|Al (100 nm) for hole-only, respectively.

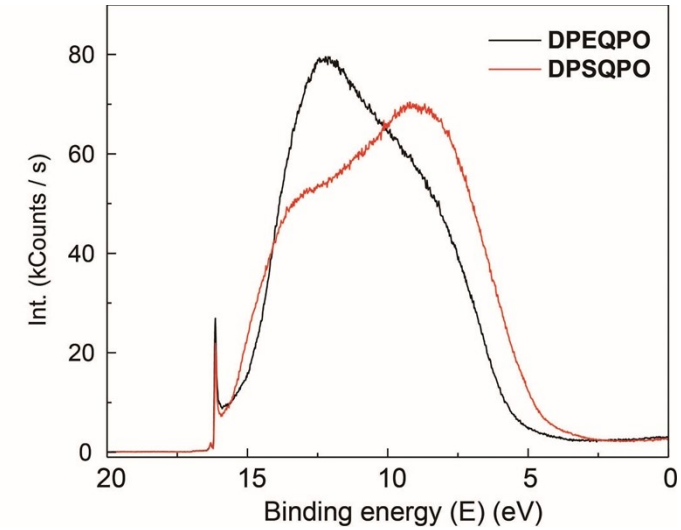

Figure S11. UPS spectra of **DPXQPO** films (100 nm).

VII. Photophysical Properties

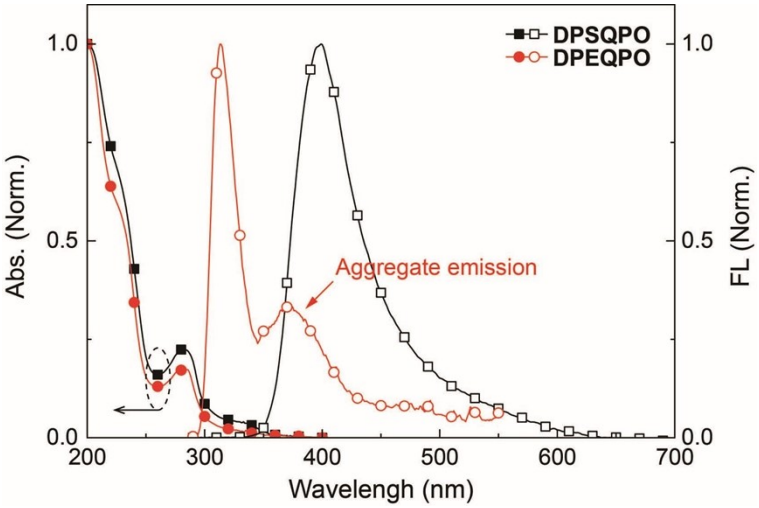

Figure S12. UV-vis absorption and FL spectra of *vacuum*-evaporated neat films for **DPXQPO** (100 nm).

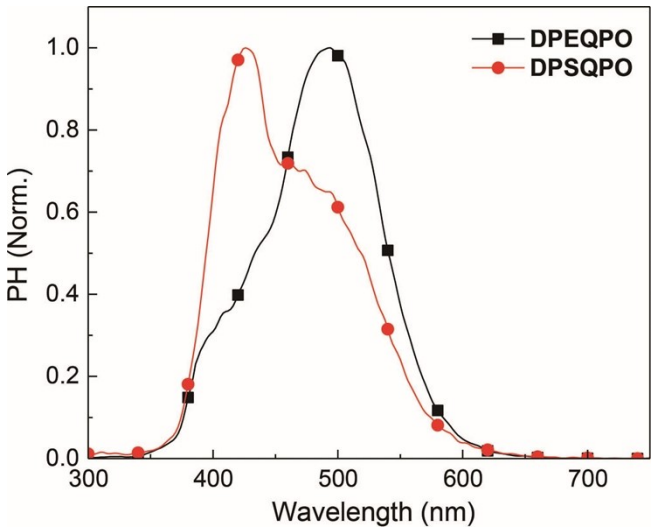

Figure S13. PH spectra of *vacuum*-evaporated neat films for **DPXQPO** (100 nm) measured with time-resolved technology after a delay of 1 ms.

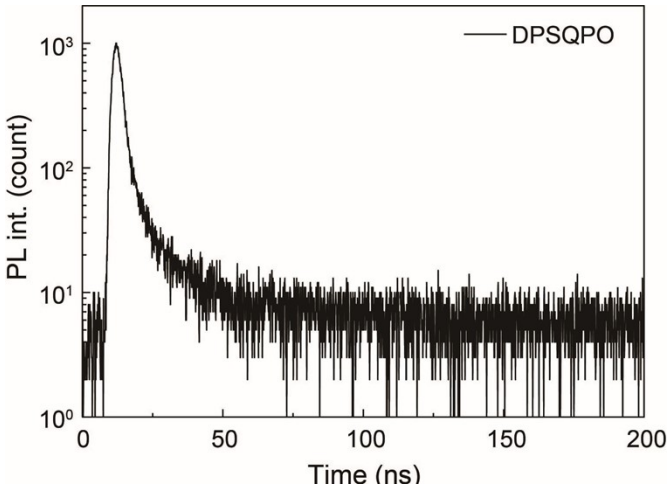

Figure S14. Emission time decay of neat **DPSQPO** films (100 nm).

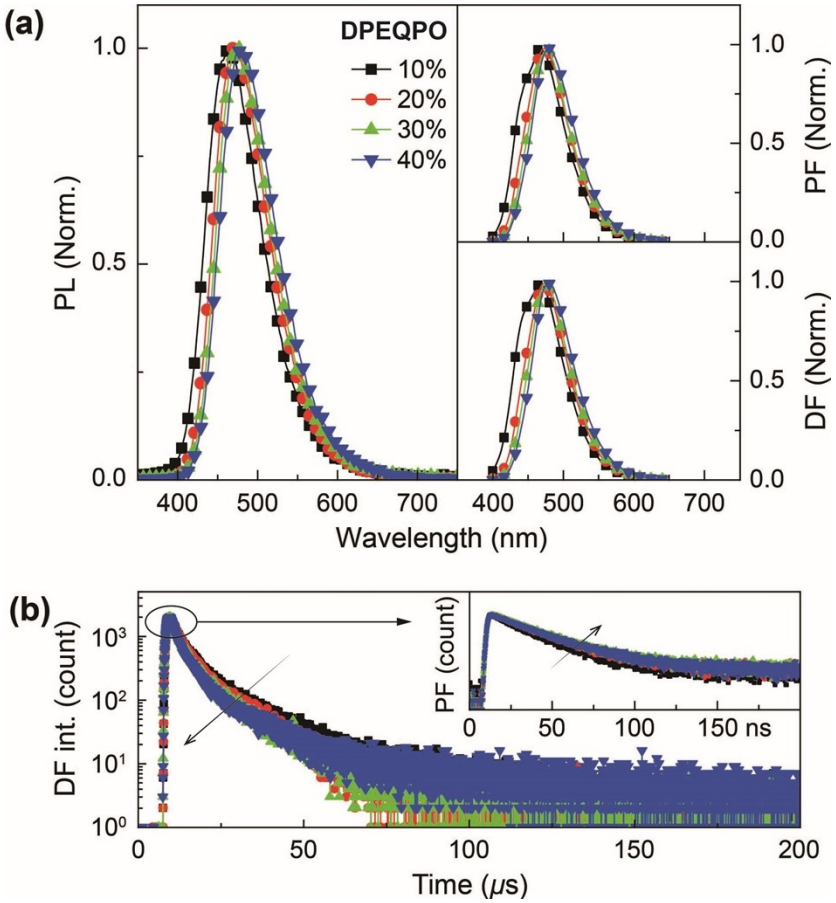

Figure S15. Dependence of (a) steady-state PL (left), PF and DF spectra and (b) PF and DF time decays on doping concentration of **DPEQPO**:*x*% DMAC-DPS films (100 nm).

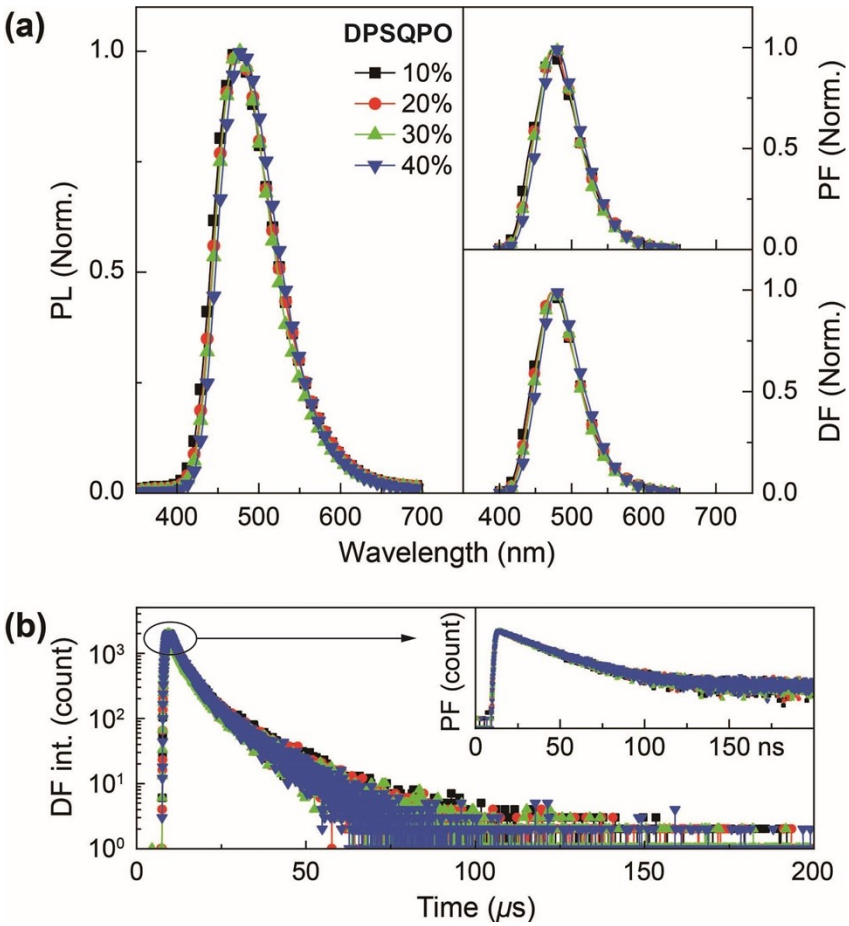

Figure S16. Dependence of (a) steady-state PL (left), PF and DF spectra and (b) PF and DF time decays on doping concentration of **DPSQPO**:*x*% DMAC-DPS films (100 nm).

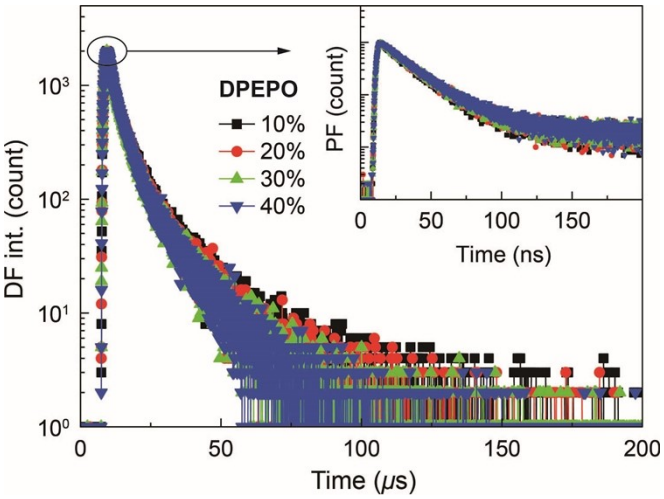

Figure S17. Dependence of PF and DF time decays on doping concentration of **DPEPO**:*x*% DMAC-DPS films (100 nm).

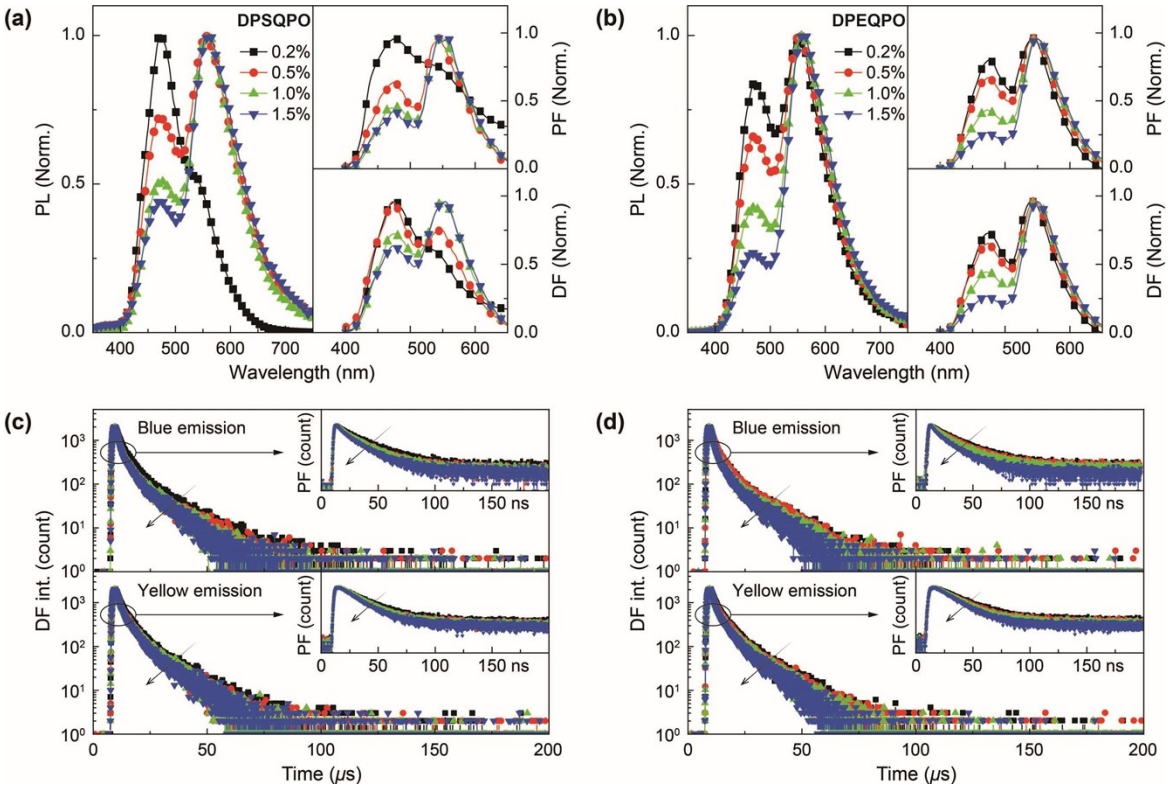

Figure S18. Dependence of (ab) steady-state PL (left), PF and DF spectra and (cd) PF and DF time decays of blue and yellow components on doping concentration of **DPSQPO**:30% DMAC-DPS:*y*% 4CzTPNBu (ac) and **DPEQPO**:30% DMAC-DPS:*y*% 4CzTPNBu (bd) films (100 nm).

Table S3. Physical Properties of **DPXQPO**.

TADF dye	λ_{Abs} (nm)	λ_{PL} (nm)	S_1 (eV)	T_1 (eV)	ΔE_{ST}[d] (eV)	f_S	T_m / T_d (°C)	HOMO (eV)	LUMO (eV)	μ_G[c] (Debye)
DPSQPO	228, 262, 326[a]	365[a]	3.02[a]	2.91[a]	0.11[a]	0.45[c]	265/427[e]	-5.72[c]	-1.32[c]	3.17[c]
	228, 282, 330[b]	399[b]	3.74[c]	3.03[b]	0.64[c]	0.24		-6.56[f]	-3.11[f]	
				3.10[c]				7.48[g]	4.46[h]	
DPEQPO	228, 262, 302[a]	311[a]	3.28[a]	2.98[a]	0.31[a]	0.05[c]	219/421[e]	-6.46[c]	-1.06[c]	10.99[c]
	232, 285 [b]	313, 370[b]	4.58[c]	3.03[b]	1.45[c]	0.16		-6.54[f]	-2.83[f]	
				3.13[c]				8.31[g]	5.03[h]	

[a] In toluene solution (10^{-6} mol L^{-1}); [b] in film; [c] Gaussian simulation results of single molecules; [d] singlet-triplet splitting; [e] temperature at weight loss of 5%; [f] calculated according to cyclic voltammetric results; [g] Ionization potential (IP) and [h] electron affinity (EA) values measured with UV photoelectronic spectra (UPS).

VIII. References

[1] J. Zhang, D. Ding, Y. Wei, F. Han, H. Xu, W. Huang, Adv. Mater. 2016, 28, 479.

[2] A. D. Becke, J. Chem. Phys. 1993, 98, 5648.

[3] C. Lee, W. Yang, R. G. Parr, Phys. Rev. B 1988, 37, 785.

[4] R. L. Martin, J. Chem. Phys. 2003, 118, 4775.